Excited-state proton transfer in protonated adrenaline revealed by cryogenic UV photodissociation spectroscopy

Jordan Dezalay, Michel Broquier, Satchin Soorkia, Keisuke Hirata, Shun-Ichi Ishiuchi, Masaaki Fujii, Gilles Grégoire

Excited-state proton transfer in protonated adrenaline revealed by cryogenic UV photodissociation spectroscopy

Received 00th January 20xx,
Accepted 00th January 20xx

DOI: 10.1039/x0xx00000x

Jordan Dezalay,[a] Michel Broquier,[a] Satchin Soorkia,[a] Keisuke Hirata,[b,c] Shun-ichi Ishiuchi,[b,c] Masaaki Fujii[b,c,d] and Gilles Grégoire*[a,d]*

We report a comprehensive study of the structures and deactivation porcesses of protonated adrenaline through cryogenic UV photodissociation spectroscopy. Single UV and double-resonance UV-UV hole burning spectroscopies have been performed and compared to coupled-cluster SCS-CC2 calculations done on the ground and first electronic states. Three conformers were assigned, the two lowest energy gauche conformers along with a higher energy conformer with an extended structure which is indeed the global minimum in solution. This demonstrates the kinetic trapping of this high energy gas phase conformer during the electrospray process. At the band origin of all conformers, the main fragmentation channel is the C_α-C_β bond cleavage, triggered by an excited state proton transfer to the catechol ring. Internal conversion leading to the water loss channel competes with the direct dissociation and tends to prevail with the increase of excess energy brought by the UV laser. Picosecond time-resolved pump-probe spectroscopy was achieved to measure the excited state lifetimes of the three conformers of AdH^+, which decay with the increase of excess in the $\pi\pi^*$ state from 2 ns at the band origin down to few hundreds of picosecond 0.5 eV to the blue. Finally, about 0.8 eV above the band origin, the $\pi\sigma^*$ state is directly reached leading to the opening of the H-loss channel.

1. Introduction

Adrenaline (Epinephrine), a human hormone belonging to the catecholamine family, is produced in response to acute stress and acts as a neurotransmitter involved in blood pressure regulation. Adrenaline binds to the α and β adrenergic receptors and activates G protein[1,2] through multiple H-bonds and proton interaction. As many neurotransmitters, adrenaline is a flexible molecule which indeed assures the molecular recognition with its receptor. The search for pharmaceutical ligands binding to those receptors can benefit from the study of the neurotransmitter flexibility, which can be precisely addressed through gas phase laser spectroscopy and quantum chemistry calculations. For instance, β-blockers bind to the adrenergic receptors and therefore inhibit the effect of adrenaline.[3] The spectroscopic study of gas phase conformers of neutral adrenaline was achieved by Carçabal et al.[4] A dominant conformer was evidenced, with an extended side-chain structure stabilized by a C_βOH to N intramolecular hydrogen bond. However, at physiological conditions, adrenaline is protonated at the methyl amino group[5] which should have a major impact on this intramolecular H-bond. Alagona et al.[6] investigated theoretically the conformational landscape of protonated adrenaline (AdH^+) both in the gas phase and in aqueous solution. Three structural families were identified, differing by a $2\pi/3$ rotation of the alkyl amino chain along the C_α-C_β bond (see chart 1). In the gauche (folded) G1 conformer, both NH to C_βOH and proton-π interactions stabilize the gas phase structure while in aqueous solution, the trans (extended) T conformer is favored, due to the high solvation energy of the protonated methyl ammonium group by water. Both structures show a preference for NH to C_βOH intramolecular hydrogen bond. The last family, in which the latter interaction is absent, the gauche G2 conformer, lies higher in energy both in the gas phase and in solution. Finally, for each family, four catechol ring orientations (STR1-4) are possible (see Chart 1) following the notation previously introduced.[6]

Structural investigation of flexible molecules in the gas phase is generally conducted through comparison of IR spectroscopy in the ground state with quantum chemistry calculations. For catecholamines, the distinct intramolecular H-bonds between protonated methyl ammonium and OH or catechol ring (gauche and trans forms) should normally provide sizeable spectral shifts that could be used for conformer assignment. However, for each of these rotamers, catechol ring orientation (STR1-4) has a little effect on the OH and NH stretching modes, precluding a definitive assignment of the structures through IR spectroscopy only. This has been recently documented for protonated noradrenaline, precursor of adrenaline in which the amine is not methylated, studied via cryogenic laser spectroscopy by Wako et al.[7] Interestingly, UV photodissociation spectroscopy of cold protonated molecules has emerged in the last decade and can nowadays be applied for structural assignment of medium size molecules through comparison with high-level excited state calculations. For instance, syn/anti conformation (position of the protonated amino group compared to the oxygen lone pair of the phenol ring) of protonated tyrosine[8] and synephrine[9] have distinct vibronic spectra although their vibrational spectra in the 3 µm

[a] *Université Paris-Saclay, CNRS, Institut des Sciences Moléculaires d'Orsay, F-91405 Orsay, France. E-mail : gilles.gregoire@universite-paris-saclay.fr*
[b] *Laboratory for Chemistry and Life Science, Institute of Innovative Research, Tokyo Institute of Technology, 4259, Nagatsuta-cho, Midori-ku, Yokohama, 226-8503, Japan. Email: mfujii@res.titech.ac.jp*
[c] *School of Life Science and Technology, Tokyo Institute of Technology. 4259 Nagatsuta-cho, Midori-ku, Yokohama, Kanagawa, 226-8503, Japan.*
[d] *Tokyo Tech World Research Hub Initiative (WRHI), Institute of Innovation Research, Tokyo Institute of Technology, 4259, Nagatsuta-cho, Midori-ku, Yokohama, 226-8503, Japan*

† Electronic Supplementary Information (ESI) available: one- and two-color photoinduced mass spectra; comparison between simulated Franck-Condon spectra of conformer G1-str3 and G1-str4; FC active modes of the four conformers; comparison between the AdH^+ vibronic spectrum recorded with the 0.2 cm^{-1} resolution dye laser and the 10 cm^{-1} resolution OPA laser; optimized structures of the $\pi\pi^*$ state and ESPT form. See DOI: 10.1039/x0xx00000x

region (NH and OH stretches) cannot be discriminated, even via cryogenic IR spectroscopy.

Beside the structural assignment of protonated molecules, UV photodissociation spectroscopy allows to decipher the deactivation processes at play following electronic excitation, where competition between internal conversion to the ground state and photoinduced reaction triggered in the excited state occurs. In particular, the specific C_α-C_β bond cleavage following UV excitation of protonated aromatic amino acids and peptides has recently been reviewed by Grégoire and coworkers.[10] Such specific photofragmentation patterns could be useful for fast screening and identify biological molecules by mass spectrometry with complementary techniques as low energy collision (CID) or electron capture dissociation (ECD).[11] Furthermore, studying protonated systems cooled at cryogenic temperature reveals possible conformer selectivity which might be of prime importance for understanding the specific molecular recognition of such flexible neurotransmitters.[12]

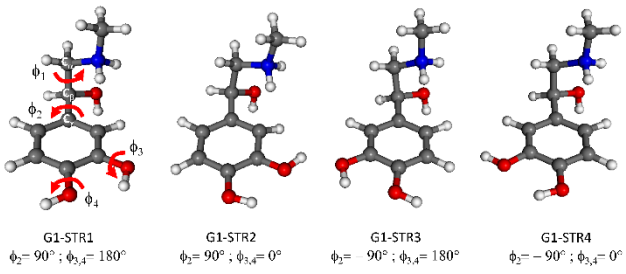

Chart 1 G1-STR1-4 structures of protonated adrenaline AdH^+. The three rotamers G1, G2 and T correspond to $\phi_1 \approx$ -60°, 60° and 180° respectively. For each rotamer, $\phi_2 \approx \pm$ 90° and $\phi_{3,4} \approx$ 0 or 180° define the different orientations of the catechol ring, noted STR1, STR2, STR3 and STR4.

In this work, the structures and conformer-resolved excited state properties of AdH^+ were investigated through cryogenic UV photodissociation spectroscopy in two laboratories. Conformer selected spectroscopies were recorded with high resolution nanosecond lasers in Tokyo, which includes UV photodissociation and UV-UV hole burning techniques. In Orsay, picosecond pump-probe photodissociation experiments were performed to record the excited state lifetime of the conformers assigned in Tokyo. We will discuss on the deactivation processes in the excited state and the evolution of the fragmentation branching ratio with the excess energy and the probed electronic state. The experimental data are analyzed by comparison with high level excited state calculations at the coupled-cluster SCS-CC2, including geometry optimization and frequency calculations.

2. Experimental and theoretical methods

The details of the experimental setup in Tokyo Institute of Technology are described elsewhere.[13] Adrenaline (purchased from Sigma Aldrich) is dissolved at 10 µM into methanol containing 0.5% formic acid. The solution is sprayed from a nebulizer, and fine droplets were drawn into glass capillary heated at 60°C. The entrance of the glass capillary is coated by metal and high voltage (-4.5 kV) is applied to it. The desolvated ions are introduced to higher vacuum region via a skimmer and guided to a quadrupole mass spectrometer (Q-MS: Extrel) by a home-made hexapole ion guide whose pole diameter is 2 mm and operated at 4 MHz (RF generator CGC). Protonated adrenaline ions, mass-selected in the Q-MS, are introduced into a cryogenic 3-dimensional quadrupole ion trap (3D-QIT) made of copper via a home-made quadrupole ion deflector and a home-made octopole ion guide (pole diameter: 4 mm, RF: 1.6 MHz). The QIT is mounted on a second stage of a double stage closed cycle He cryostat (Sumitomo: RDK-408D2) cooled at 4 K. At the exit of the octopole ion guide, there is a pulsed lens electrode (20 Hz) to chop the ion beam to introduce the ions into the cryogenic QIT during 35 ms. He buffer gas at room temperature is introduced just before the entering of the ions and cooled down by collisions with the copper electrodes of the QIT. The trapped ions are thermalized at ~ 13 K by the cold He buffer gas.[13] Then, a tunable UV laser (probe laser) is triggered at 37 ms and the photo fragments are ejected at 40 ms and detected by a home-made time of flight mass spectrometer (TOF-MS). The TOF-MS signal is amplified 10 times by a preamplifier (NF: BX-31A) and recorded by a fast digitizer board (NI: PXIe-5160) as a function of the wavelength of the UV laser.

To measure UV-UV hole burning (UV-UV HB) spectra, another tunable UV laser (burn laser) is introduced to the cryogenic QIT 1 ms before the probe laser. During this 1 ms, a tickle RF pulse[7,13,14] is applied to the entrance end-cup of the QIT to eject photo fragments produced by the burn laser. UV-UV HB spectra are recorded by monitoring the photo fragment signal due to the probe laser whose wavelength is fixed to a given band of the UVPD spectrum while scanning the wavelength of the burn laser. When the wavelength of the burn laser is resonant to any electronic transitions of the probed conformer, a decrease of ion signal is observed, which reflects depopulation of the zero vibrational level of this specific conformer. The probe laser is operated at 20 Hz, while the burn laser at 10 Hz. Therefore, probe-laser-only signal and double resonance signal were obtained alternatively. By dividing the latter by the former, long term fluctuations of the source condition, etc. could be cancelled.[15]

The setup installed in Orsay has already been described in details.[16] AdH^+ ions are produced in an electrospray source, first stored in an octopole ion trap for 100 ms and then extracted and accelerated at 200 V by a pulsed exit electrode and finally transferred in the cold 3D-QIT (Jordan Tof Inc.). The latter is biased at 200 V to ensure efficient trapping and avoid collision induced dissociation of the incoming ions with He buffer gas injected by a pulsed valve 1-2 ms before. The 3D-QIT is housed in a copper box directly mounted on a cold head of a compressed helium cryostat (CH-204 S, Sumitomo) that maintains the temperature around 15 K. A pulsed mass gate located before the entrance of the trap allows for mass-selecting the parent ion. The photodissociation laser is triggered at least 40 ms after the trapping of the ions when thermalization is achieved and helium buffer gas is mostly pumped. All ionic fragments and parent molecules are then extracted and accelerated for mass-analysis in a linear time-of-flight mass

spectrometer and detected by MCP (Z-Gap, Jordan Tof Inc.). Fragmentation time can be recorded from 1 µs up to tens of ms by varying the delay between the photofragmentation laser and the extraction of the ions from the QIT.

The photodissociation UV laser (pump) is the output of an optical parametric amplifier (EKSPLA-PG411) pumped by the third harmonic (355 nm) of a mode-locked picosecond Nd-YAG laser (EKSPLA-SL300) operated at 10 Hz which provides tunable visible/UV light in the 740-220 nm region. The spectral resolution is in the order of 8-10 cm^{-1}. For the 2 color experiments, the probe laser is the output of a second OPA pumped with the same laser. The probe laser has been scanned in the visible range without noticeable change and has been set at 550 nm. The picosecond time-resolved photodissociation spectroscopy[17] is recorded by delaying the probe laser beam with a motorized optical delay line with 6.6 ps time step and a maximum delay time of 1.4 ns. Both beams are mildly focused by a 700 mm lens and cross each other in the center of the trap. Typical laser pulse energies are in the order of 40 µJ for the pump and 200 µJ for the probe beam. The cross correlation of the picosecond lasers is about 16 ps.

Ab initio calculations have been performed with the TURBOMOLE program package[18] (v6.6) making use of the resolution-of-the-identity (RI) approximation for the evaluation of the electron-repulsion integrals.[19,20] The equilibrium geometries of AdH^+ in its electronic ground (S_0) and excited (S_1 and S_2) states have been determined at the CC2 level[21,22] with the correlation-consistent polarized valence double-ζ aug-cc-pVDZ basis set augmented with diffuse functions.[23] In particular, the spin-component scaled approach (SCS) was applied since it improves the accuracy of CC2 calculations for the charge transfer states.[24] The vibrational modes of the ground and the first excited states have been calculated at the same level in order to obtain the adiabatic excitation energy corrected for the difference of zero-point energy between the two states. The calculated vibrationally-resolved electronic spectra were obtained with the PGOPHER spectra simulator package[25] using the calculated frequencies of the ground and excited states. For sake of comparison, the simulation was performed at 0 K and convoluted with a gaussian function of 3 cm^{-1} (full-width at half-maximum FWHM).

3. Results and discussion

3. 1. Conformer assignment: UV photodissociation and UV-UV hole-burning spectra

The UV photodissociation mass spectrum of protonated adrenaline AdH^+ (m/z 184) shown in Fig. S1 corresponds to the difference mass spectrum (UV laser – no laser) with a delay between the laser excitation and the extraction of the ions from the QIT of 1 µs. In that conditions, only the fast fragmentation events are detected. The fragmentation channels can be sorted in two main groups. As for Noradrenaline,[26] the m/z 166 fragment corresponds to the water loss channel which is the main dissociation channel in the ground electronic state obtained through low energy collision and can eventually further fragment into its secondary fragment at m/z 135 (H_2O + NH_2CH_3 loss) at longer fragmentation time. The other prompt fragmentation channels are issued from the C_α-C_β bond cleavage with the charge on the catechol ring (m/z 139) or on the amino alkyl chain moieties (m/z 46 and m/z 44) following H/H+ rearrangement. The last fragmentation channel at m/z 32 is assigned to the $NH_3CH_3^+$ ionic fragment (C_α-N bond break). It should be stressed here that such fragmentation pattern, competition between CID like fragments and specific UV fragments issued from the C_α-C_β bond break,[10] is commonly observed in the UV photodissociation of protonated aromatic amines,[27] amino acids,[28–31] catecholamine[7] and short peptides.[32–37] As it can be readily seen in Fig. S1, the fragmentation branching ratio is larger for the C_α-C_β bond cleavage events than for internal conversion.

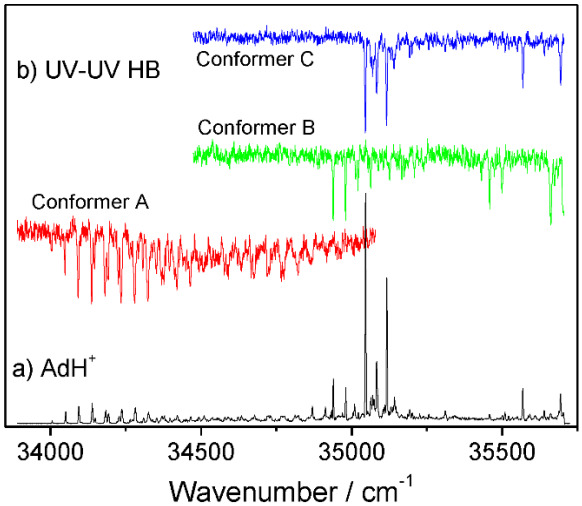

Fig. 1 (a) UV photodissociation spectrum and (b) UV-UV hole burning spectra of AdH^+ recorded on the m/z 139 channel issued from the C_α-C_β bond cleavage.

The electronic spectroscopy of AdH^+ reported in Fig. 1a has been recorded on the C_α-C_β bond cleavage fragment (m/z 139). The spectrum closely resembles the noradrenaline ($NAdH^+$) one.[7] The first weak vibronic transition is detected at 34 004 cm^{-1} along with a long progression of low-frequency mode of 45 cm^{-1} which extends up to hundreds of wavenumbers to the blue. Two sets of intense transitions are observed at 34 938 cm^{-1} and 35 046 cm^{-1}, which indeed correspond to the band origins of two other conformers as revealed by the UV-UV hole-burning spectroscopy reported in Fig. 1b. In this spectral region from 34 000 to 35 800 cm^{-1}, the excitation spectrum of AdH^+ is thus composed of three different conformers.

Ab initio excited state calculations at the SCS-CC2/aug-cc-pVDZ level have been performed to assign the structure of the three conformers of AdH^+. Following the same notation as for $NAdH^+$, the conformers of AdH^+ can be sorted in three main families (G1, G2 and T) according to the 2π/3 rotamers along the C_α-C_β bond.[6] The G1-STR1 conformer, in which the protonated $CH_3NH_2^+$ group is involved in two H-bonds with the catechol ring and the C_β-OH group, is the lowest energy minimum (see Chart 1). In this form, the protonated group is in syn position as compared to the oxygen lone pair of the hydroxyl groups of the

catechol ring, above the OH group in meta position. The G1-STR3 conformer, iso energetic with G1-STR1, corresponds to an inversion of the $C_\alpha C_\beta C_\gamma C$ ϕ_2 dihedral angle, so the NH_2 group is no more on the top of the catechol OHs. For each conformer, the CCOH $\phi_{3,4}$ dihedral angle of the catechol OHs can be inverted (G1-STR2 and G1-STR4, respectively) but their relative energies are significantly higher by 2.1 kcal/mol and 1.2 kcal/mol. In the T structures, the NH_2 group forms a sole H-bond with the $C_\beta OH$ group in a trans orientation compared to the catechol ring ($\phi_1 \approx 180°$). Such rotamers are among the lowest energy ones in aqueous solution[6,38] but in the gas phase, due to the lack of proton-π interaction, only the T-STR1 conformer has a relative low energy. Finally, all the conformers of the third rotamer family G2 ($\phi_1 \approx 60°$), in which the NH_2 group is not involved in H-bond with the $C_\beta OH$ group, have relative energies much higher and can be discarded from the analysis.

Table 1: Conformer assignment, relative energy (kcal/mol) in the ground state E_{S0}, calculated and experimental π–π* adiabatic excitation energy 0_0^0 with the absolute error $\Delta^{calc-exp}$ (cm^{-1}).

	Structure	E_{S0}	0_0^0 (calc)	0_0^0 (exp)	$\Delta^{calc-exp}$
Conf. A	G1-STR1	0	33 296	34 004	- 707
Conf. B	T-STR1	1.8	34 274	34 938	- 663
Conf. C	G1-STR3	0	34 470	35 046	- 575
	G1-STR4	1.2	34 310		

In Table 1 are reported the ground state relative energies and π-π* adiabatic excitation energies of the most relevant conformers of AdH^+. Conformer A has the reddest band origin, almost 1000 cm^{-1} below those of conformers B and C. The adiabatic excitation energy calculated for G1-STR1 is significantly lower than for all the other conformers. Its simulated Franck-Condon spectrum is reported in Fig. 2a and provides a fair agreement with the experimental spectrum of conformer A. Accordingly, conformer B of AdH+ can be confidently assign to the T-STR1 structure, giving the good agreement with the adiabatic excitation energy and the simulated vibronic spectrum (Fig. 2b). The extended structure T, in which the protonated methyl amino group does not interact with the catechol ring, lies relatively high in energy in the gas phase and should not be populated in the cold ion trap, unless kinetic trapping of the AdH^+ most stable solution phase structure occurs, as already observed in $NAdH^+$.[7] Finally, conformer C is tentatively assigned to structure G1-STR3, although we cannot exclude the structure G1-STR4 which both provide satisfying adiabatic energy transitions and simulated FC spectra (Fig. 2c and Fig. S2). The active modes of the vibronic spectra of the 4 conformers are depicted in Fig. S3-6. One should stress here that for these two latter conformers, the intensity of the vibronic transitions 200 cm^{-1} above the band origin is significantly reduced compared to the predicted one while two intense bands show up at 523 cm^{-1} and 649 cm^{-1}. Such a cut-off was already observed in $NAdH^+$, structure G1-STR3.[7] We do not have a simple explanation although this cut-off occurs for the same type of structure. Finally, it is worth mentioning that the absolute error in adiabatic excitation energies is quite low, less than 2%, which is totally consistent with the absolute error found at the CC2 level for protonated aromatic amino acids and related systems. In overall, the conformational landscape of AdH^+ and $NAdH^+$ are similar, although more conformers were observed for $NAdH^+$

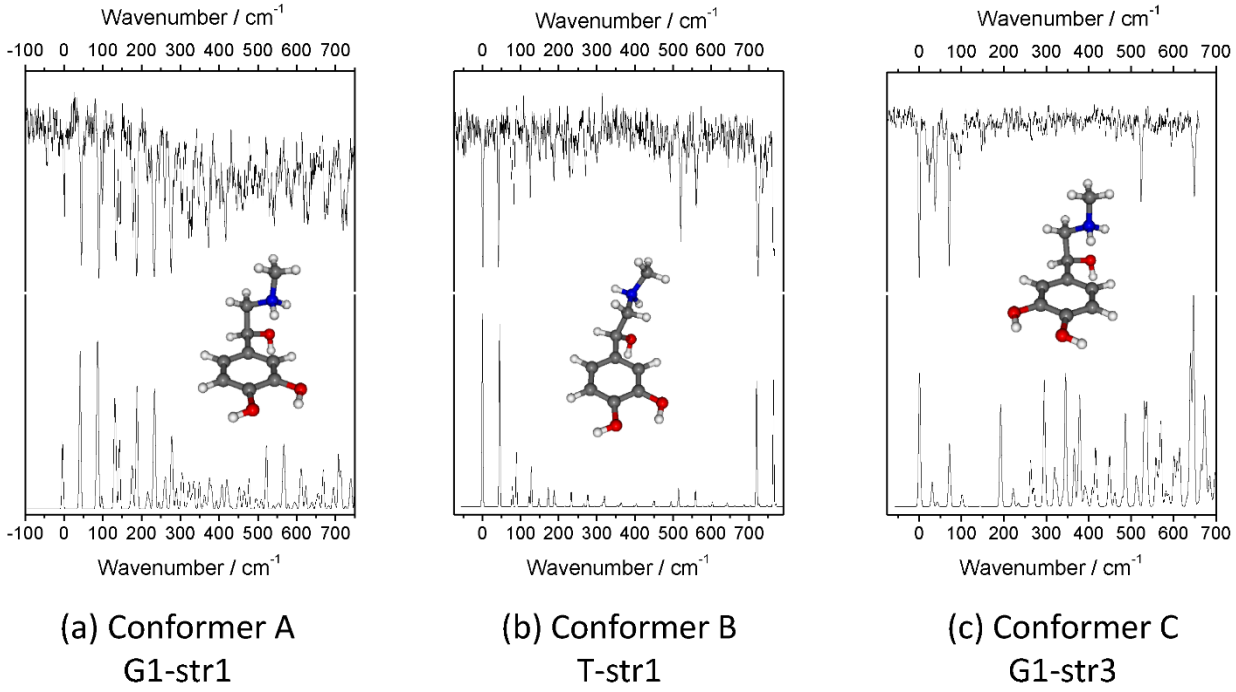

Fig. 2 Conformer assignment of AdH^+ through comparison between the experimental and simulated vibronic spectra.

3.2. Excited State lifetime

The excited state lifetimes of AdH^+ have been recorded through a picosecond pump-probe photodissociation scheme. In Fig. SI7, the vibronic spectrum recorded with the low resolution OPA picosecond laser is compared to the higher resolution spectrum (dye laser). The band origins of the three conformers A, B and C are readily observed along with the main vibronic transitions except for conformer B for which only the origin transition is clearly observed. So the pump-probe photodissociation dynamics have been monitored as a function of the pump excess energy for the two gauche conformers A and C and only at the band origin of the trans conformer B. In the two-color excitation scheme with the probe laser set at 550 nm, the photofragmentation pattern changes, with the opening of the H-loss channel at m/z 183 along with an net increase of the m/z 44, which is indeed the main fragment of the adrenaline radical cation. The difference mass spectrum (two-color excitation versus UV pump only) is reported in Fig. S2b. All the fragmentation channels observed through UV excitation are depleted following absorption of the probe beam, whatever the probe wavelength used in the visible from 420 nm to 650 nm or set at 355 nm. In Fig. 3a and Fig. 3b are reported the transients recorded on the H loss channel, average of the m/z 183 and m/z 44 signals, for the conformers A and C excited on the 0_0^0 transition and about 800 cm^{-1} further to the blue. In Fig. 3c, the dynamics recorded at the band origin of conformer B is plotted.

All the transients have been fitted by a mono exponential decay function with a time constant τ convoluted by a gaussian function to take into account the temporal profile of the picosecond lasers (autocorrelation of 16 ps). The average uncertainty on the time constant issued from the fitting process is about 10-20 %. All conformers behave essentially the same with an excited state lifetime of about 2 ns, which smoothly decreases with the increase of excess energy imparted by the pump laser. It should be noted that at much higher pump energy, i.e. 37 000 cm^{-1} (270 nm), the time constant is significantly shorter, in the order of 370 ps (Fig. 3d), but consistent with an exponential decay of the excited state lifetime with the increase of excess energy.

The excited state lifetime of AdH^+, in the order of 2 ns at the band origin, is significantly longer than in neutral catechol (about 10 ps)[39] for which the lifetime is governed by strong coupling of the locally excited $^1\pi\pi^*$ with the dissociative $^1\pi\sigma_{OH}^*$ state along the O-H stretch. This coupling is strongly disturbed in water and crown ether complexes as revealed by the elongated lifetime of 10-12 ns.[40] Interestingly, the lifetime of AdH^+ is similar to the lifetimes recorded for similar systems, such as protonated tyrosine[17] or tyramine.[16] In these latter systems, excited state proton transfer process was clearly evidenced as the main deactivation process near the band origin while electronic coupling with charge transfer states ($\pi\sigma^*$ or $\pi\pi_{CO}^*$) prevails higher in energy. As it will be discussed below, this general deactivation mechanism applied to AdH^+.

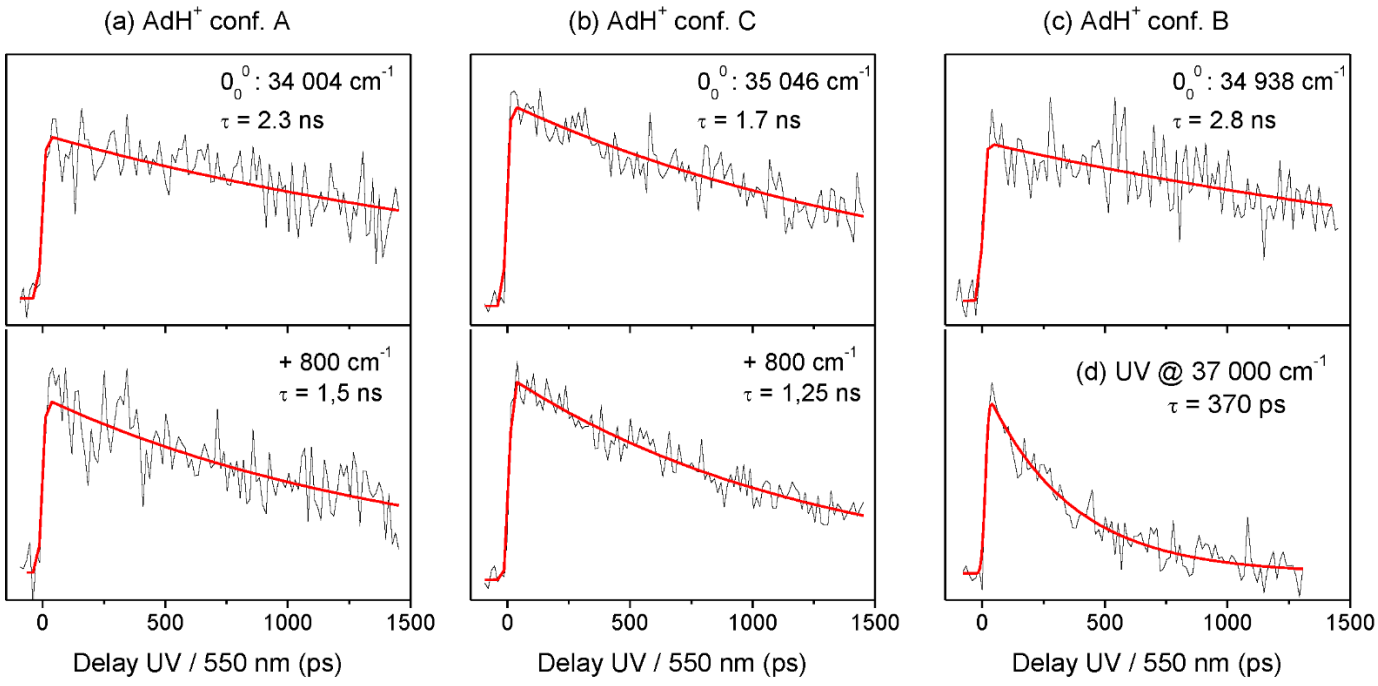

Fig. 3 (a-c) Excited state lifetime of the three conformers of AdH+ (conformers A, C and B, respectively) as a function of the excitation wavelength recorded on the H-loss channel. The red curve is a monoexponential decay fitting function with a time constant τ, reflecting the excited state lifetime of the probed conformer at a given vibronic level. (d) pump wavelength set at 270 nm from which the C_α-C_β bond cleavage fragmentation channel closes.

3.3. Deactivation mechanism

3.3.1. C_α-C_β bond cleavage triggered by excited state proton transfer ESPT. Two main photodissociation channels are in competition following electronic excitation of AdH+ (m/z 184) at the band origin of the π-π* transition. The first one corresponds to water loss (m/z 166), which is the primary and first dissociation channel at low energy in the ground state, which eventually further dissociates into m/z 135 (H_2O and NH_2CH_3 loss). The other photofragments are specific to UV excitation and are related to the C_α-C_β bond cleavage. Depending on the final localization of the charge, such bond break can lead to the ionic fragment m/z 139 (hole on the catechol ring) plus the neutral alkyl amino chain moieties at 45 Da, or inversely to the ionic m/z 46 (hydrogenated m/z 45 cation) or m/z 44 (dehydrogenated m/z 45 cation). All these primary fragmentation events happen on a short time scale, within less than 1 µs, as it can be seen in Fig S1.

In Fig. 4 is reported the evolution of the fragmentation yields of the C_α-C_β bond cleavage, the water loss and the H loss on a large spectral range from the band origin of conformer A (34 000 cm^{-1}, 4.2 eV) up to 45 000 cm^{-1} (5.6 eV). These spectra have been recorded with the OPA ps laser at a low spectral resolution. In Fig. SI 7, we compare the spectroscopy recorded on the m/z 139 fragment with the nanosecond (0.2 cm^{-1} resolution) and picosecond (10 cm^{-1} resolution). The main difference is the broad continuum obtained with the ps laser beneath the sharp vibronic transitions assigned to conformer A and C, which might be due to spectral congestion that cannot be accurately recorded with the OPA laser. Such broadening precludes the observation of all the transitions except the band origin assigned to the extended conformer B (around 34 900 cm^{-1}) with the ps laser, which are nevertheless clearly detected with a 0.2 cm^{-1} dye laser.

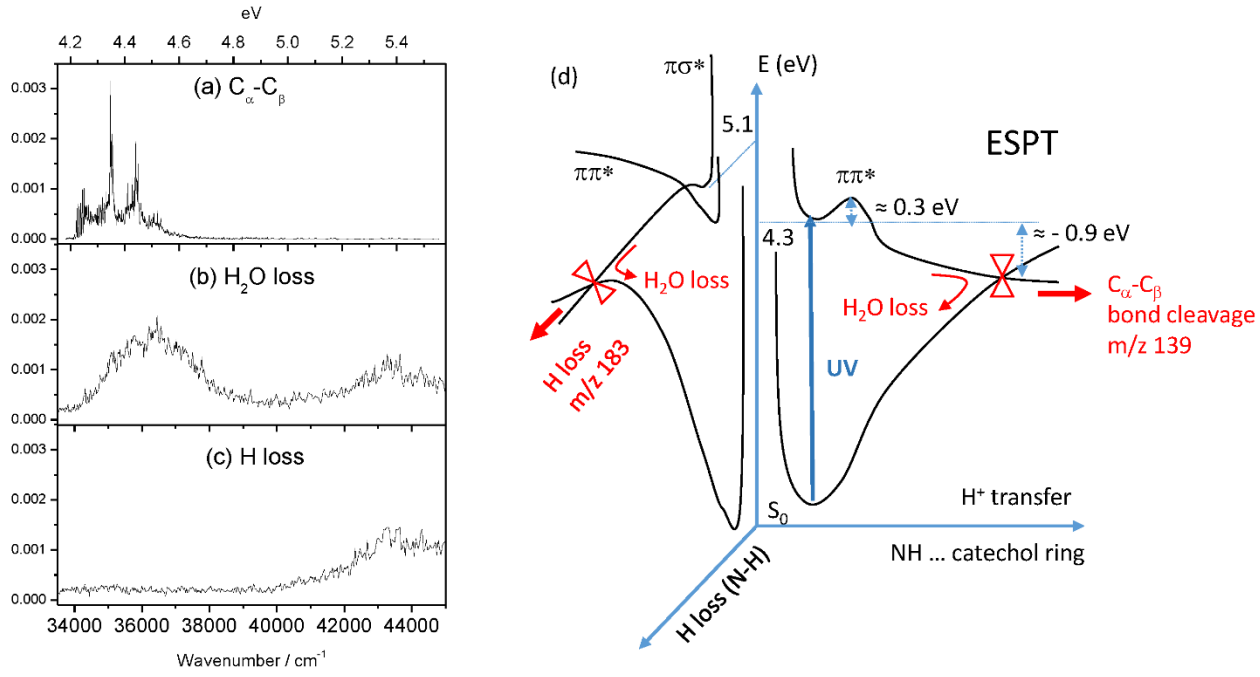

Fig. 4 Fragmentation yields of AdH^+ recorded on (a) C_α-C_β bond break, (b) H_2O loss and (c) H loss on a large spectral range from the band origin of the π–π* transition up to 1.3 eV above. The fragmentation yields are plotted on the same vertical scale for sake of comparison. (d) Schematic representation of the PESs along the proton transfer coordinate and the H loss along the NH coordinate.

The C_α-C_β bond cleavage occurs at the band origin of the ππ* state in all conformers. Such photoinduced reaction has previously been assigned in aromatic amines, amino acids and related systems such as synephrine to excited state proton transfer from the ammonium group to the aromatic ring.[10] In the optimized structure of the ππ* state of conformer A, a lengthening of the N-H bond (0.023 Å) pointing to the ring along with an out-of-plane bending of the CH (≈30°) facing the protonated group are observed (see Fig. S8). The Minimum Energy Path (MEP) for the excited state proton transfer reaction has been evaluated at the SCS-CC2/aug-cc-pVDZ level, i.e. optimization of the first excited state at fixed N-H bond lengths. It should be stressed here that full optimization of the transferred form in the excited state leads to a curve crossing with the ground state, point where the optimization at the CC2 level fails to converge. So, in the course of the proton transfer reaction, a direct C_α-C_β bond cleavage is expected to occur, in competition with internal conversion leading to H_2O loss, as it will be discussed below. A barrier for ESPT of 0.30 eV at NH=1.4 Å has been found, quite similar to the one calculated for

synephrine[9] and twice larger than for tyrosine.[28,31] In these two latter systems, the ionic photo fragment associated to C_α-C_β bond cleavage has the aromatic ring with an extra proton and/or hydrogen attached to it, consistent with the proton transfer process. For AdH^+, the fragment at m/z 139 corresponds to the ionic catechol ring following C_α-C_β bond rupture. This suggests that hydrogen rearrangement occurs after the initial proton transfer, as confirmed by the detection of two ionic fragments at m/z 44 and 46 (alkyl amino chain counterpart of the catechol ring).

3.3.2. Reaction path connecting the T and G1 conformers in the excited state. In the trans T-STR1 structure (conformer B), the methyl ammonium group does not interact with the catechol ring, so direct proton transfer can obviously not occur, although the C_α-C_β bond cleavage reaction is indeed observed (Fig. 1). We have calculated the reaction path connecting the two trans (T-STR1) and gauche (G1-STR1) structures in the excited state at the CC2-SCS/aug-cc-pVDZ. Fourteen intermediate structures were used for discretization of the path, which have been optimized throughout, leading to an energy barrier of 0.1 eV from the trans to the gauche conformer (see Fig. 5). Such a low energy transition state connecting the two rotamers could be overcome within the nanosecond excited state lifetime of the $\pi\pi^*$ state.

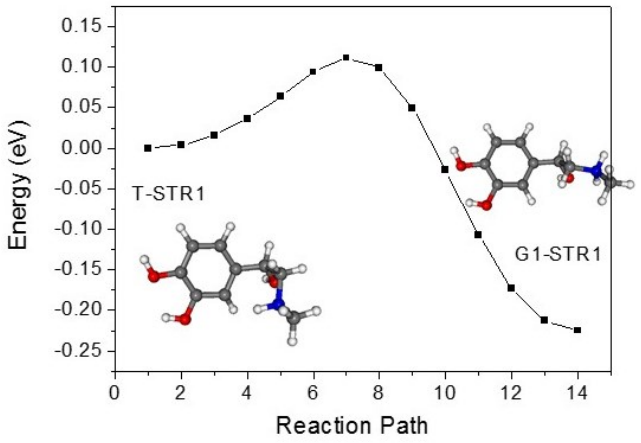

Fig. 5 Excited state reaction path connecting the trans (T-STR1) and gauche (G1-STR1) structures of AdH^+.

3.3.3. Competition between C_α-C_β bond cleavage and water loss. At the band origin of conformer A (34 004 cm-1), the C_α-C_β bond break channels are more intense than the water loss channel, but the spectroscopy recorded on both is similar, with a bell shape structure of low frequency modes. Interestingly, the fragmentation branching ratio drastically evolves with the excess energy in the excited state, the spectroscopy recorded on the water loss fragment exhibits a broad, unstructured absorption band centred at 37 000 cm-1. From this excitation energy, the C_α-C_β bond cleavage channel closes.

The mechanism leading to water loss indeed remains unclear. Water loss is the main dissociation channel in the ground state at low excitation energy, so internal conversion to the ground state is thought to be responsible for its detection following UV excitation. In the course of the excited state proton transfer, the S_1/S_0 energy gap vanishes so internal conversion could occur, in competition with the prompt C_α-C_β bond cleavage (see Fig. 4). In that case, the photodissociation spectroscopy recorded on both fragments (m/z 166 and m/z 139) should be similar, reflecting the absorption of AdH^+. This is indeed what happens at the band origin of all conformers. In the spectral region of the band origins of conformer B and C, conformer A still absorbs but the fragmentation branching ratio seems to evolve in favor of the water loss channel. The 0_0^0 transitions of conformer B and C are clearly detected on the m/z 139 fragment (background free) but buried in the water loss channel due to the contribution of the high energy absorption band of conformer A. Note that with the better spectral resolution provided by the dye laser, the band origin of these two latter conformers are observed at the m/z 166 fragment on the top of a broad fragmentation continuum. Such changes in the fragmentation branching ratio with the excess energy has already been observed and rationalized in protonated phenylethylamine and tyramine.[27] C_α-C_β bond cleavage is the main or unique fragmentation channel at the band origin and closes few hundreds wavenumbers to the blue when ammonia loss, issued from internal conversion to the ground state, becomes the unique fragmentation channel. Conformer A (G1-STR1) of AdH^+ shares the same property, internal conversion to the ground state prevails as the excess energy in the $\pi\pi^*$ state increases, leading to the broad absorption band detected on the water loss channel.

3.3.4. Opening of the H loss channel. The onset of a second absorption band is clearly observed from 40 000 cm^{-1}, *i.e.* about 0.75 eV above the adiabatic excitation energy of the $\pi\pi^*$ state, with the opening of the H loss and H_2O loss channels. The opening of the H loss channel 1 eV or less above the onset of the π–π^* transition has already been observed and assigned to the direct excitation of the $\pi\sigma^*$ state.[41–43] Vertical and adiabatic energies of the $\pi\sigma^*$ state have been calculated for the three AdH^+ conformers and the results are reported in Table 2. In all conformers, the S_2 $\pi\sigma_{NH2}^*$ state lies 0.6-0.8 eV above the S_1 $\pi\pi^*$ state at the ground state geometry (vertical excitation energy). Optimization of the S_2 $\pi\sigma^*$ state leads to a true minimum (no imaginary frequency) of the potential energy surface for the gauche conformers A and C, with an adiabatic transition energy 0.73 eV and 0.61 eV above the band origin of the S_1 $\pi\pi^*$ state, respectively. For the trans structure T-STR1 (conformer B), $\pi\sigma^*$ geometry optimization leads to a curve crossing with the $\pi\pi^*$ state, 0.57 eV above its band origin. At this point, the optimization is restarted on the S_1 electronic state but because of the large mixing of the π^* and σ^* orbitals in the electronic configuration of the state, the optimization finally converges to the minimum of the $\pi\pi^*$ electronic state. The lower transition energy of the $\pi\sigma^*$ state in the trans conformer can be qualitatively explained by the absence of proton-π interaction in this structure, the σ_{NH2}^* orbital being destabilized when the protonated group is involved in two H-bonds like in the gauche conformers. Finally, it is worth noting that the calculated $\pi\sigma^*$

adiabatic energy transition matches the onset of the second absorption band of AdH^+ leading to the H loss fragment about 0.75 eV above the onset of the $\pi-\pi^*$ transition.

Table 2 Vertical and adiabatic excitation energy of the $\pi\pi^*$ and $\pi\sigma^*$ states of the three AdH^+ conformers. Adiabatic energy corrected by the difference in zero point energy in the ground and excited states. All values in eV.

Structure	$\pi\pi^*/\pi\sigma^*$ vert. energy	$\pi\pi^*/\pi\sigma^*$ adiab. energy	$\Delta\ \pi\sigma^*/\pi\pi^*$ adiab. energy
G1-STR1 - conf A	4.52 / 5.35	4.13 / 4.87	0.73
G1-STR3 - conf C	4.61 / 5.30	4.27 / 4.88	0.61
T-STR1 - conf B	4.63 / 5.14	4.25 / 4.82[a]	0.57[a]

[a] energy at the crossing point with $\pi\pi^*$ state, not a true minimum

Such charge transfer state in which the anti-bonding orbital is centred on the protonated amino group is dissociative through a barrier along the N-H stretch coordinate and will cross the ground electronic state (see Fig. 4). Since the H-loss ionic fragment is detected, it can be concluded that the $\pi\sigma^*/S_0$ curve crossing occurs at a lower energy than the excitation energy, otherwise hindered H-loss reaction leading to internal conversion would happen.[27] The fragmentation yield on the H_2O loss channel increases as well in the same spectral region, meaning that part of the population following the dissociative $\pi\sigma^*$ surface will go back to the ground state at the $\pi\sigma^*/S_0$ crossing. It is noteworthy that the deactivation through the dissociative $\pi\sigma^*$ state does not induce the C_α-C_β bond cleavage, since this latter fragmentation channel is not observed along with the H loss channel. So in overall, the nonradiative deactivation processes in AdH^+ involves proton transfer to the aromatic ring at the band origin while the coupling with the $^1\pi\sigma_{NH2}^*$ charge transfer state prevails about 0.7 eV higher in energy. This mechanism is also found in protonated tyrosine and may be general for protonated catecholamines.

4. Conclusions

We have reported the UV photodissociation spectroscopy of cold AdH^+. Three conformers have been identified through comparison of the UV-UV hole burning spectra with high-level calculations at the SCS-CC2 level in the ground and excited states. As for $NAdH^+$, the relatively high energy trans conformer T, in which the alkyl side chain is in anti orientation compared to the catechol ring is observed, reflecting the kinetic trapping of this structure initially present in solution during the ESI process. The excited state lifetimes of the gauche and trans conformers have been determined around 2 ns at the band origin and smoothly decrease with the excess energy in the locally excited $\pi\pi^*$ state. Interestingly, the main deactivation process at the band origin of all AdH^+ conformers is the excited state proton transfer to the catechol ring, leading mostly to C_α-C_β bond cleavage fragments. In the ESPT structure, the S_1/S_0 energy gap vanishes so competition between direct C_α-C_β bond cleavage and internal conversion occurs. It turns out that internal conversion to the ground state leading to water loss prevails with the increase of excess energy in the $\pi\pi^*$ state. Less than 1 eV above the $\pi\pi^*$ state, direct excitation of the $\pi\sigma^*$ state is evidenced by the opening of the H-loss channel.

Conflicts of interest

There are no conflicts to declare.

Acknowledgements

This work was supported in part by the ANR Research Grant (ANR2010BLANC040501-ESPEM), by KAKENHI (JP19H05527, JP18H01938, JP19K23624) of JSPS, World Research Hub Initiatives in Tokyo Institute of Technology, the Cooperative Research Program of the "Network Joint Research Center for Materials and Devices" from the Ministry of Education, Culture, Sports, Science and Technology (MEXT), Japan, and the RIKEN Pioneering Project, "Fundamental Principles Underlying the Hierarchy of Matter: A Comprehensive Experimental Study". GG thanks the Tokyo Institute of Technology for the invited professor grant. We also acknowledge the use of the computing facilities Méso-LUM of the LUMAT federation (LUMAT FR 2764) and MAGI of University Paris 13.

References

1 F. Fanelli and P. G. De Benedetti, Computational Modeling Approaches to Structure−Function Analysis of G Protein-Coupled Receptors, *Chem. Rev.*, 2005, **105**, 3297–3351.

2 T. Warne, R. Moukhametzianov, J. G. Baker, R. Nehmé, P. C. Edwards, A. G. W. Leslie, G. F. X. Schertler and C. G. Tate, The structural basis for agonist and partial agonist action on a β1-adrenergic receptor, *Nature*, 2011, **469**, 241–245.

3 O. Ramström, C. Yu and K. Mosbach, Chiral Recognition in Adrenergic Receptor Binding Mimics Prepared by Molecular Imprinting, *J. Mol. Recognit.*, 1996, **9**, 691–696.

4 P. Çarçabal, L. C. Snoek and T. Van Mourik, A computational and spectroscopic study of the gas-phase conformers of adrenaline, *Mol. Phys.*, 2005, **103**, 1633–1639.

5 R. Álvarez-Diduk and A. Galano, Adrenaline and noradrenaline: Protectors against oxidative stress or molecular targets?, *J. Phys. Chem. B*, 2015, **119**, 3479–3491.

6 G. Alagona and C. Ghio, Competitive H-bonds in vacuo and in aqueous solution for N-protonated adrenaline and its monohydrated complexes, *J. Mol. Struct. THEOCHEM*, 2007, **811**, 223–240.

7 H. Wako, S. Ishiuchi, D. Kato, G. Féraud, C. Dedonder-Lardeux, C. Jouvet and M. Fujii, A conformational study of protonated noradrenaline by UV–UV and IR dip double resonance laser spectroscopy combined with an electrospray and a cold ion trap method, *Phys. Chem. Chem. Phys.*, 2017, **19**, 10777–10785.

8 J. A. Stearns, S. Mercier, C. Seaiby, M. Guidi, O. V. Boyarkin and T. R. Rizzo, Conformation-Specific Spectroscopy and Photodissociation of Cold, Protonated Tyrosine and

Phenylalanine, *J. Am. Chem. Soc.*, 2007, **129**, 11814–11820.
9 N. Nieuwjaer, C. Desfrançois, F. Lecomte, B. Manil, S. Soorkia, M. Broquier and G. Grégoire, Photodissociation Spectroscopy of Cold Protonated Synephrine: Surprising Differences between IR–UV Hole-Burning and IR Photodissociation Spectroscopy of the O–H and N–H Modes, *J. Phys. Chem. A*, 2018, **122**, 3798–3804.
10 S. Soorkia, C. Jouvet and G. Grégoire, UV Photoinduced Dynamics of Conformer-Resolved Aromatic Peptides, *Chem. Rev.*, 2020, **120**, 3296–3327.
11 R. Antoine, M. Broyer, C. Dedonder, C. Desfrancois, C. Jouvet, D. Onidas, P. Poulain, T. Tabarin, P. Dugourd, G. Gregoire and G. Van Der Rest, Comparison of the fragmentation pattern induced by collisions , laser excitation and electron capture . Influence of the initial excitation, *Rapid Commun. Mass Spectrom.*, 2006, **20**, 1648–1652.
12 T. Sekiguchi, M. Tamura, H. Oba, P. Çarçarbal, R. R. Lozada-Garcia, A. Zehnacker-Rentien, G. Grégoire, S. Ishiuchi and M. Fujii, Molecular Recognition by a Short Partial Peptide of the Adrenergic Receptor: A Bottom-Up Approach, *Angew. Chemie*, 2018, **130**, 5728–5731.
13 S. Ishiuchi, H. Wako, D. Kato and M. Fujii, High-cooling-efficiency cryogenic quadrupole ion trap and UV-UV hole burning spectroscopy of protonated tyrosine, *J. Mol. Spectrosc.*, 2017, **332**, 45–51.
14 H. Kang, G. Féraud, C. Dedonder-Lardeux and C. Jouvet, New Method for Double-Resonance Spectroscopy in a Cold Quadrupole Ion Trap and Its Application to UV–UV Hole-Burning Spectroscopy of Protonated Adenine Dimer, *J. Phys. Chem. Lett.*, 2014, **5**, 2760–2764.
15 Y. Okuzawa, M. Fujii and M. Ito, Direct observation of second excited 1,3 (n,π*) states of pyrazine by UV-IR double resonance dip spectroscopy, *Chem. Phys. Lett.*, 1990, **171**, 341–346.
16 M. Broquier, S. Soorkia and G. Grégoire, A comprehensive study of cold protonated tyramine: UV photodissociation experiments and ab initio calculations, *Phys. Chem. Chem. Phys.*, 2015, **17**, 25854–25862.
17 S. Soorkia, M. Broquier and G. Grégoire, Conformer- and Mode-Specific Excited State Lifetimes of Cold Protonated Tyrosine Ions, *J. Phys. Chem. Lett.*, 2014, **5**, 4349–4355.
18 *TURBOMOLE V6.6, a Dev. Univ. Karlsruhe Forschungszentrum Karlsruhe GmbH, 1989-2007, TURBOMOLE GmbH, since 2007; available from http//www.turbomole.com.*
19 O. Christiansen, H. Koch and P. Jørgensen, The second-order approximate coupled cluster singles and doubles model CC2, *Chem. Phys. Lett.*, 1995, **243**, 409–418.
20 R. Ahlrichs, Efficient evaluation of three-center two-electron integrals over Gaussian functions, *Phys. Chem. Chem. Phys.*, 2004, **6**, 5119.
21 C. Hättig, Geometry optimizations with the coupled-cluster model CC2 using the resolution-of-the-identity approximation, *J. Chem. Phys.*, 2003, **118**, 7751–7761.
22 A. Köhn and C. Hättig, Analytic gradients for excited states in the coupled-cluster model CC2 employing the resolution-of-the-identity approximation, *J. Chem. Phys.*, 2003, **119**, 5021–5036.
23 R. A. Kendall, T. H. Dunning and R. J. Harrison, Electron affinities of the first-row atoms revisited. Systematic basis sets and wave functions, *J. Chem. Phys.*, 1992, **96**, 6796–6806.
24 A. Hellweg, S. A. Grün and C. Hättig, Benchmarking the performance of spin-component scaled CC2 in ground and electronically excited states, *Phys. Chem. Chem. Phys.*, 2008, **10**, 4119.
25 C. M. Western, PGOPHER: A program for simulating rotational, vibrational and electronic spectra, *J. Quant. Spectrosc. Radiat. Transf.*, 2017, **186**, 221–242.
26 F. Rogalewicz, S. Bourcier and Y. Hoppilliard, Decomposition of protonated noradrenaline and normetanephrine assisted by NH2 migration studied by electrospray tandem mass spectrometry and molecular orbital calculations, *Rapid Commun. Mass Spectrom.*, 2005, **19**, 743–751.
27 G. Féraud, M. Broquier, C. Dedonder-Lardeux, G. Grégoire, S. Soorkia and C. Jouvet, Photofragmentation spectroscopy of cold protonated aromatic amines in the gas phase, *Phys. Chem. Chem. Phys.*, 2014, **16**, 5250–5259.
28 G. Grégoire, C. Jouvet, C. Dedonder and A. L. Sobolewski, Ab initio Study of the Excited-State Deactivation Pathways of Protonated Tryptophan and Tyrosine, *J. Am. Chem. Soc.*, 2007, **129**, 6223–6231.
29 B. Lucas, M. Barat, J. A. Fayeton, M. Perot, C. Jouvet, G. Grégoire and S. Brondsted Nielsen, Mechanisms of photoinduced Calpha-Cbeta bond breakage in protonated aromatic amino acids., *J. Chem. Phys.*, 2008, **128**, 164302.
30 G. Grégoire, B. Lucas, M. Barat, J. A. Fayeton, C. Dedonder-Lardeux and C. Jouvet, UV photoinduced dynamics in protonated aromatic amino acid, *Eur. Phys. J. D*, 2009, **51**, 109–116.
31 G. Féraud, M. Broquier, C. Dedonder, C. Jouvet, G. Grégoire and S. Soorkia, Excited State Dynamics of Protonated Phenylalanine and Tyrosine: Photo-Induced Reactions Following Electronic Excitation, *J. Phys. Chem. A*, 2015, **119**, 5914–5924.
32 C. Dehon, S. Soorkia, M. Pedrazzani, C. Jouvet, M. Barat, J. A. Fayeton and B. Lucas, Photofragmentation at 263 nm of small peptides containing tyrosine: the role of the charge transfer on CO, *Phys. Chem. Chem. Phys.*, 2013, **15**, 8779.
33 A. V. Zabuga, M. Z. Kamrath, O. V. Boyarkin and T. R. Rizzo, Fragmentation mechanism of UV-excited peptides in the gas phase, *J. Chem. Phys.*, 2014, **141**, 154309.
34 S. Soorkia, C. Dehon, S. K. S, M. Pérot-Taillandier, B. Lucas, C. Jouvet, M. Barat and J. A. Fayeton, Ion-Induced Dipole Interactions and Fragmentation Times: Cα-Cβ Chromophore Bond Dissociation Channel, *J. Phys. Chem. Lett.*, 2015, **6**, 2070–2074.
35 N. L. Burke, J. G. Redwine, J. C. Dean, S. A. McLuckey and T. S. Zwier, UV and IR spectroscopy of cold protonated leucine enkephalin, *Int. J. Mass Spectrom.*, 2015, **378**, 196–205.
36 V. Kopysov, A. Makarov and O. V. Boyarkin, Nonstatistical

UV Fragmentation of Gas-Phase Peptides Reveals Conformers and Their Structural Features, *J. Phys. Chem. Lett.*, 2016, **7**, 1067–1071.

37 A. F. DeBlase, C. P. Harrilal, J. T. Lawler, N. L. Burke, S. A. McLuckey and T. S. Zwier, Conformation-Specific Infrared and Ultraviolet Spectroscopy of Cold [YAPAA+H] + and [YGPAA+H] + Ions: A Stereochemical "Twist" on the β-Hairpin Turn, *J. Am. Chem. Soc.*, 2017, **139**, 5481–5493.

38 H. Wang, Z. Huang, T. Shen and L. Guo, Hydrogen-bonding interactions in adrenaline-water complexes: DFT and QTAIM studies of structures, properties, and topologies, *J. Mol. Model.*, 2012, **18**, 3113–3123.

39 R. A. Livingstone, J. O. F. Thompson, M. Iljina, R. J. Donaldson, B. J. Sussman, M. J. Paterson and D. Townsend, Time-resolved photoelectron imaging of excited state relaxation dynamics in phenol, catechol, resorcinol, and hydroquinone, *J. Chem. Phys.*, 2012, **137**, 184304.

40 F. Morishima, R. Kusaka, Y. Inokuchi, T. Haino and T. Ebata, Anomalous cage effect of the excited state dynamics of catechol in the 18-crown-6-catechol host-guest complex, *J. Phys. Chem. B*, 2015, **119**, 2557–2565.

41 H. Kang, C. Dedonder-Lardeux, C. Jouvet, S. Martrenchard, G. Grégoire, C. Desfrançois, J.-P. Schermann, M. Barat and J. A. Fayeton, Photo-induced dissociation of protonated tryptophan TrpH + : A direct dissociation channel in the excited states controls the hydrogen atom loss, *Phys. Chem. Chem. Phys.*, 2004, **6**, 2628–2632.

42 H. Kang, C. Dedonder-Lardeux, C. Jouvet, G. Grégoire, C. Desfrançois, J.-P. Schermann, M. Barat and A. Fayeton, Control of Bond-Cleaving Reactions of Free Protonated Tryptophan Ion by Femtosecond Laser Pulses, *J. Phys. Chem. A*, 2005, **109**, 2417–2420.

43 H. Kang, C. Jouvet, C. Dedonder-Lardeux, S. Martrenchard, G. Grégoire, C. Desfrançois, J.-P. Schermann, M. Barat and J. a. Fayeton, Ultrafast deactivation mechanisms of protonated aromatic amino acids following UV excitation, *Phys. Chem. Chem. Phys.*, 2005, **7**, 394.